

Decoupling Networks and Super-Quadratic Gains for RIS Systems with Mutual Coupling

Dominik Semmler, Josef A. Nossek, *Life Fellow, IEEE*, Michael Joham, Benedikt Böck, and Wolfgang Utschick, *Fellow, IEEE*

School of Computation, Information and Technology, Technical University of Munich, 80333 Munich, Germany
email: {dominik.semmler,josef.a.nossek,joham,benedikt.boeck,utschick}@tum.de

Abstract—We propose decoupling networks for the reconfigurable intelligent surface (RIS) array as a solution to benefit from the mutual coupling between the reflecting elements. In particular, we show that when incorporating these networks, the system model reduces to the same structure as if no mutual coupling is present. Hence, all algorithms and theoretical discussions neglecting mutual coupling can be directly applied when mutual coupling is present by utilizing our proposed decoupling networks. For example, by including decoupling networks, the channel gain maximization in RIS-aided single-input single-output (SISO) systems does not require an iterative algorithm but is given in closed form as opposed to using no decoupling network. In addition, this closed-form solution allows to analytically analyze scenarios under mutual coupling resulting in novel connections to the conventional transmit array gain. In particular, we show that super-quadratic (up to quartic) channel gains w.r.t. the number of RIS elements are possible and, therefore, the system with mutual coupling performs significantly better than the conventional uncoupled system in which only squared gains are possible. We consider diagonal as well as beyond diagonal (BD)-RISs and give various analytical and numerical results, including the inevitable losses at the RIS array. In addition, simulation results validate the superior performance of decoupling networks w.r.t. the channel gain compared to other state-of-the-art methods.

Index Terms—Decoupling Networks, Legendre Polynomials

I. INTRODUCTION

RISs are currently highly discussed as they are considered an important technology for future wireless communications systems (see [2], [3]). RISs are arrays consisting of many passive reflecting elements which can manipulate the incoming wavefronts and, hence, shape the propagation environment. The potential of RISs has already been demonstrated and utilizing a RIS has shown to significantly improve, e.g., power consumption [2] and energy efficiency [4] in various scenarios. In these publications each of the reflecting elements is modeled by a phase manipulation. This model is the most popular and is used in the majority of the RIS literature (see [5]–[12]).

The architecture of RIS arrays is still under research and various approaches are discussed, including simultaneously transmitting and reflecting (STAR) RISs [13], [14], active RISs [15], [16] as well as BD-RISs [17]–[19]. For BD-RISs, the manipulation matrix at the RIS is not restricted to be diagonal but is generalized to a non-diagonal matrix allowing

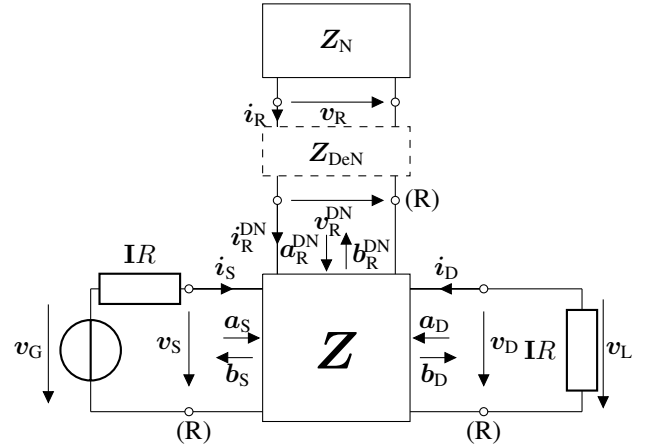


Fig. 1. Multiport Model of [20] with an additional decoupling network Z_{DeN} .

the different elements to be connected with each other (see [17]). This leads to an improved performance at the cost of having an increased complexity. Regardless of the chosen architecture, the elements at the RIS are typically mounted on a surface close to each other. Hence, mutual coupling between the RIS elements is inevitable in such a system. The effect of coupling between the elements is usually neglected, however, the system performs very differently when mutual coupling is included. When including mutual coupling, a more advanced RIS model is needed in comparison to the phase-shift model.

Modeling the RIS is under ongoing research and different models for RISs have already been proposed in the literature. In, e.g., [21], a RIS model has been introduced that is based on impedance matrices. Impedance-based descriptions have already been shown to provide a powerful description for conventional communication systems without the RIS (see [22]). The model in [21] allows to include the effect of mutual coupling as well as different RIS architectures. Furthermore, in [17], the RIS has been modeled based on scattering parameters which can also include the effects of mutual coupling (see [23]). Both models describe the same electromagnetic system and, hence, lead to the same conclusions. A comparison of these two models is given in [20], [24]–[26] and with the correct interpretation of the matrices (see [20]), both approaches are equivalent.

It is therefore possible to use both, the scattering, as

Preliminary results have been presented at the ISWCS 2024 [1].

well as the impedance formulation to model the RIS system under mutual coupling and one can also switch between the two descriptions when modeling the system. When mutual coupling is included in the system model, both, the scattering and the impedance descriptions become intricate and the system optimization and analysis gets more complicated. For example, in [27], mutual coupling has been analyzed based on impedance matrices and an algorithm using the Neumann series has been proposed for maximizing the SISO channel gain. The impact of mutual coupling on the rate has been further investigated in [28] and [29]. Additionally, in [24], two mutual coupling aware algorithms based on the scattering parameters have been proposed which outperform the method in [27]. All these algorithms rely on the Neumann series approximation whereas in [30], an element-wise algorithm has been derived which requires no approximation and provides closed-form solutions for each reactance. In our previous work [1], we propose an element-wise algorithm with reduced complexity. All these solutions require an iterative algorithm to optimize the system under mutual coupling even in the simple case of maximizing a single-user SISO channel gain. Furthermore, as the solution with coupling requires an iterative algorithm it is difficult to analytically analyze the system. Mutual coupling has also been investigated for the BD-RIS in [23] based on the Neumann series. Similarly, the solution provided in this work also requires an iterative algorithm.

In our conference paper [1], we propose decoupling networks as a solution to benefit from the mutual coupling at the RIS array. These networks have already been well investigated for the conventional transmit array (see, e.g., [22]). In [1], we demonstrate that the decoupling network transforms the system into a structure which is equivalent to a system without mutual coupling for which the coupling matrices are transferred into the channel matrices. This simplifies the system model drastically as the model without coupling is significantly easier to handle and, additionally, well understood. A direct consequence is that all methods (algorithms as well as theoretical analyses) without mutual coupling can be directly applied to the case of mutual coupling by incorporating decoupling networks into the model. For example, the solution of a single-user SISO channel gain maximization without mutual coupling can be given in closed-form [27]. Hence, by using decoupling networks, a closed-form solution exists even in the case when considering mutual coupling (see [1]). This has led to an analytical analysis of mutual coupling in [1] and we have shown that super-quadratic gains are possible under mutual coupling.

The resulting channel structure due to the decoupling networks which we have introduced in our conference paper [1] has recently been applied to analyze the BD-RIS with mutual coupling [31].

In this article, we extend our results of [1] providing a thorough analysis of decoupling networks for the RIS array. In particular, we provide the following contributions:

- Decoupling networks are proposed to handle the mutual coupling in the RIS array. We show that when including

these networks, the structure of the system model reduces to the case of no mutual coupling. Hence, all conventional solutions, neglecting the mutual coupling, can be directly extended to the case of mutual coupling when incorporating our proposed decoupling networks. This comprises all algorithms as well as theoretical analyses.

- With decoupling networks, the equivalent adjustable impedance network obtains a non-diagonal structure even when considering a single-connected RIS. While the equivalent matrix is non-diagonal, our method is significantly different to BD-RISs in which non-diagonal adjustable impedance networks are also used. Hence, we provide a thorough comparison of the approaches and highlight their differences.
- With decoupling networks it is possible to optimize the channel gain of a RIS-aided SISO system in closed form which allows to analytically analyze the array gain of a RIS array under mutual coupling. From this analysis, we can draw connections to the conventional transmit array gain. In particular, we prove that a super-quadratic array gain which scales with N^4 is possible in a RIS-aided scenario. In fact, this result provides novel insights in RIS-aided communication since in previous work, it was assumed that only quadratic gains (i.e., N^2) are possible. Additionally, we compare the decoupling networks to the conventional RIS (with and without mutual coupling) and show under which conditions the decoupling network is optimal. Furthermore, the important case of $\frac{\lambda}{2}$ antenna spacing is investigated.
- With the decoupling networks, we analyze both the single-connected RIS as well as the BD-RIS under mutual coupling and show that regardless of the user position the BD-RIS channel gain scales at least cubic. Furthermore, we show that including losses in the model significantly impacts the system's performance
- We demonstrate that the proposed decoupling networks result in superior performance w.r.t. the channel gain compared to other state-of-the-art methods.

II. SYSTEM MODEL

We consider a RIS-aided point-to-point multiple-input multiple-output (MIMO) system where one base station (BS), having M antennas, transmits data signals to K receive antennas. The transmission is supported by a RIS, consisting of N reflecting elements. By using the impedance representation, the channel from the BS to the receiver reads as (see [21], [20])

$$\begin{aligned} \mathbf{v}_L &= \mathbf{D}\mathbf{v}_G = \frac{1}{4R}\mathbf{Z}\mathbf{v}_G \quad \text{with} \\ \mathbf{Z} &= \mathbf{Z}_{\text{DS}} - \mathbf{Z}_{\text{DR}}(\mathbf{Z}_R + \mathbf{Z}_N)^{-1}\mathbf{Z}_{\text{RS}} \end{aligned} \quad (1)$$

with the definition of \mathbf{v}_G and \mathbf{v}_L according to Fig. 1. Here, \mathbf{Z}_{DS} is the direct channel from the BS to the user, \mathbf{Z}_{DR} is the channel from the RIS to the user, and \mathbf{Z}_{RS} the channel from the BS to the RIS. The adjustable passive impedance network of the RIS is given by \mathbf{Z}_N , whereas \mathbf{Z}_R is the impedance matrix of the RIS antenna array accounting for mutual coupling. If

there were no mutual coupling present, $\mathbf{Z}_R = \mathbf{I}R$ would be a diagonal matrix. In this article, we analyze the aspects of mutual coupling. For isotropic radiators (which we consider in this article), the matrix \mathbf{Z}_R is defined as (see [20, Eqn. (5)])

$$[\mathbf{Z}_R]_{i,j} = -\frac{R}{jk d |i-j|} e^{-jkd|i-j|} \quad \text{for } i \neq j, \quad (2)$$

where $k = \frac{2\pi}{\lambda}$ is the wave number and d is the element spacing in wavelengths. The diagonal entries are given by $[\mathbf{Z}_R]_{i,i} = R$. Throughout this article, we assume the adjustable impedance network \mathbf{Z}_N to be lossless and reciprocal and, hence, the matrix \mathbf{Z}_N

$$\mathbf{Z}_N = j\mathbf{X}_N \quad (3)$$

with $\mathbf{X}_N = \mathbf{X}_N^T \in \mathbb{R}^{N \times N}$ is real-valued.

III. DECOUPLING NETWORKS

To handle the mutual coupling between the reflecting elements at the RIS, we propose decoupling networks. These networks are well studied for the transmit and receive arrays (see, e.g., [22]) for handling the coupling between the antenna elements. In addition to the transmit and receive arrays, we are now also assuming a decoupling network at the RIS array according to Fig. 1. The performance of the decoupling networks for handling the mutual coupling in the RIS array is analyzed in the following.

A. Equivalent Adjustable Impedance Network

In this section, we derive the new channel model when incorporating a decoupling network \mathbf{Z}_{DeN} for the RIS array according to Fig. 1. Please note that $\mathbf{Z}_{\text{DeN}} = \mathbf{Z}_{\text{DeN}}^T$ and $\text{Re}(\mathbf{Z}_{\text{DeN}}) = \mathbf{0}$ holds as the decoupling network is assumed to be reciprocal and lossless. Without the decoupling network, the reconfigurable network can be described by the equation

$$\mathbf{v}_R = -\mathbf{Z}_N \mathbf{i}_R. \quad (4)$$

Including now the decoupling network according to Fig. 1 leads to the new relationship

$$\mathbf{v}_R^{\text{DN}} = -\mathbf{Z}_N^{\text{DN}} \mathbf{i}_R^{\text{DN}}. \quad (5)$$

In the following, we derive \mathbf{Z}_N^{DN} . With the decoupling network \mathbf{Z}_{DeN} , we obtain

$$\begin{bmatrix} \mathbf{v}_R \\ \mathbf{v}_R^{\text{DN}} \end{bmatrix} = \begin{bmatrix} \mathbf{Z}_{\text{DeN},11} & \mathbf{Z}_{\text{DeN},12} \\ \mathbf{Z}_{\text{DeN},12}^T & \mathbf{Z}_{\text{DeN},22} \end{bmatrix} \begin{bmatrix} \mathbf{i}_R \\ -\mathbf{i}_R^{\text{DN}} \end{bmatrix} \quad (6)$$

with the four $N \times N$ matrix blocks $\mathbf{Z}_{\text{DeN},ij}$. Substituting (4) into the first line of (6), we obtain

$$\mathbf{i}_R = (\mathbf{Z}_{\text{DeN},11} + \mathbf{Z}_N)^{-1} \mathbf{Z}_{\text{DeN},12} \mathbf{i}_R^{\text{DN}}. \quad (7)$$

Together with the second line of (6), we arrive at

$$\mathbf{v}_R^{\text{DN}} = -(\mathbf{Z}_{\text{DeN},22} - \mathbf{Z}_{\text{DeN},12}^T (\mathbf{Z}_{\text{DeN},11} + \mathbf{Z}_N)^{-1} \mathbf{Z}_{\text{DeN},12}) \mathbf{i}_R^{\text{DN}}. \quad (8)$$

Therefore, we have found the new matrix [cf. (5)]

$$\mathbf{Z}_N^{\text{DN}} = \mathbf{Z}_{\text{DeN},22} - \mathbf{Z}_{\text{DeN},12}^T (\mathbf{Z}_{\text{DeN},11} + \mathbf{Z}_N)^{-1} \mathbf{Z}_{\text{DeN},12} \quad (9)$$

with the new channel model [cf. (1)]

$$\mathbf{Z}^{\text{DN}} = \mathbf{Z}_{\text{DS}} - \mathbf{Z}_{\text{DR}} (\mathbf{Z}_R + \mathbf{Z}_N^{\text{DN}})^{-1} \mathbf{Z}_{\text{RS}}. \quad (10)$$

Comparing this channel model with the conventional one in (1), we can see that the adjustable impedance network \mathbf{Z}_N is replaced by \mathbf{Z}_N^{DN} of (9) due to the decoupling network. Therefore, a decoupling network only changes the adjustable impedance network by transforming the original impedance network \mathbf{Z}_N into \mathbf{Z}_N^{DN} . With a decoupling network \mathbf{Z}_{DeN} , we can now manipulate the adjustable impedance network \mathbf{Z}_N for the channel in (10) by choosing properly designed matrices in (9). Various choices exist for decoupling networks, see, e.g., [22]. The only restriction is that the network should be lossless and reciprocal, i.e., $\mathbf{Z}_{\text{DeN}} = \mathbf{Z}_{\text{DeN}}^T$ and $\text{Re}(\mathbf{Z}_{\text{DeN}}) = \mathbf{0}$. However, there is one particular network structure which allows to completely decouple the RIS array. This is the power matching network (see [22, (103)]) given by

$$\mathbf{Z}_{\text{DeN}} = -j \begin{bmatrix} \mathbf{0} & \sqrt{R} \text{Re}(\mathbf{Z}_R)^{\frac{1}{2}} \\ \sqrt{R} \text{Re}(\mathbf{Z}_R)^{\frac{1}{2}} & \text{Im}(\mathbf{Z}_R) \end{bmatrix} \quad (11)$$

with $\text{Re}(\mathbf{Z}_R) = \text{Re}(\mathbf{Z}_R)^{\frac{1}{2}} \text{Re}(\mathbf{Z}_R)^{\frac{1}{2}}$ and we particularly focus on this choice throughout this article. By using the power matching network, we arrive at the new adjustable impedance matrix

$$\mathbf{Z}_N^{\text{DN}} = -j \text{Im}(\mathbf{Z}_R) + R \text{Re}(\mathbf{Z}_R)^{\frac{1}{2}} \mathbf{Z}_N^{-1} \text{Re}(\mathbf{Z}_R)^{\frac{1}{2}}. \quad (12)$$

From (12) we can see that a lossless and reciprocal adjustable impedance network \mathbf{Z}_N directly results in a lossless and reciprocal \mathbf{Z}_N^{DN} as we have $\text{Re}(\mathbf{Z}_N^{\text{DN}}) = \mathbf{0}$ and $\mathbf{Z}_N^{\text{DN}} = \mathbf{Z}_N^{\text{DN},T}$. This property results from the assumption that the decoupling network is also lossless and reciprocal. Furthermore, we can see that even if we assume a diagonal RIS and, hence, the original impedance network \mathbf{Z}_N is diagonal, the new impedance matrix \mathbf{Z}_N^{DN} is in general non-diagonal. A non-diagonal impedance network is typically referred to the so called BD-RISs. Hence, the combination of an impedance network together with the decoupling network, resulting in a non-diagonal \mathbf{Z}^{DN} , can be viewed as a particular type of BD-RIS. However, significant differences exist when comparing them to the conventional BD-RIS architecture. Please see Section IV for details.

B. Channel Model with Decoupling Networks

In the following, we derive the new channel model when incorporating a decoupling network. We start by rewriting the matrix $\mathbf{Z}_R + \mathbf{Z}_N^{\text{DN}}$ within the inverse in (10). By inserting the definition of the new adjustable impedance network according to (12) we arrive at

$$\begin{aligned} \mathbf{Z}_R + \mathbf{Z}_N^{\text{DN}} &= \mathbf{Z}_R - j \text{Im}(\mathbf{Z}_R) + R \text{Re}(\mathbf{Z}_R)^{\frac{1}{2}} \mathbf{Z}_N^{-1} \text{Re}(\mathbf{Z}_R)^{\frac{1}{2}} \\ &= \text{Re}(\mathbf{Z}_R) + R \text{Re}(\mathbf{Z}_R)^{\frac{1}{2}} \mathbf{Z}_N^{-1} \text{Re}(\mathbf{Z}_R)^{\frac{1}{2}} \\ &= \text{Re}(\mathbf{Z}_R)^{\frac{1}{2}} (R \mathbf{I} + R^2 \mathbf{Z}_N^{-1}) \frac{1}{R} \text{Re}(\mathbf{Z}_R)^{\frac{1}{2}}. \end{aligned} \quad (13)$$

Hence, by defining the equivalent impedance network

$$\bar{\mathbf{Z}}_N = R^2 \mathbf{Z}_N^{-1} \quad (14)$$

as well as the effective impedance matrices as

$$\bar{\mathbf{Z}}_{\text{DR}} = \mathbf{Z}_{\text{DR}} \text{Re}(\mathbf{Z}_{\text{R}})^{-\frac{1}{2}} \sqrt{R}, \quad \bar{\mathbf{Z}}_{\text{RS}} = \sqrt{R} \text{Re}(\mathbf{Z}_{\text{R}})^{-\frac{1}{2}} \mathbf{Z}_{\text{RS}}, \quad (15)$$

we arrive at the new channel model

$$\begin{aligned} \mathbf{Z}^{\text{DN}} &= \mathbf{Z}_{\text{DS}} - \mathbf{Z}_{\text{DR}}(\mathbf{Z}_{\text{R}} + \mathbf{Z}_{\text{N}}^{\text{DN}})^{-1} \mathbf{Z}_{\text{RS}} \\ &= \mathbf{Z}_{\text{DS}} - R \mathbf{Z}_{\text{DR}} \text{Re}(\mathbf{Z}_{\text{R}})^{-\frac{1}{2}} (\mathbf{I}R + R^2 \mathbf{Z}_{\text{N}}^{-1})^{-1} \text{Re}(\mathbf{Z}_{\text{R}})^{-\frac{1}{2}} \mathbf{Z}_{\text{RS}} \\ &= \mathbf{Z}_{\text{DS}} - \bar{\mathbf{Z}}_{\text{DR}} (\mathbf{I}R + \bar{\mathbf{Z}}_{\text{N}})^{-1} \bar{\mathbf{Z}}_{\text{RS}} \end{aligned} \quad (16)$$

which has the same structure as a RIS channel model without mutual coupling. Therefore, this is the same structure as the conventional channel model in (1) with the difference that instead of the non-diagonal \mathbf{Z}_{R} the scaled identity $\mathbf{I}R$ is within the inverse. The effect of mutual coupling is transformed into the new channel matrices $\bar{\mathbf{Z}}_{\text{DR}}$ and $\bar{\mathbf{Z}}_{\text{RS}}$. This reduces the complexity of mutual coupling to the conventional system model without mutual coupling and all algorithms and methods can be extended to the case of mutual coupling by using these decoupling networks.

Before we focus on the analysis of this newly derived channel model, we give an alternative model based on the scattering parameters of the adjustable impedance model. This alternative representation with the scattering parameters is more popular in the literature and often leads to a representation which is easier to optimize. Hence, we switch to the scattering description of the adjustable network \mathbf{Z}_{N} leading to

$$\mathbf{Z}_{\text{N}} = R(\mathbf{I} + \Theta)(\mathbf{I} - \Theta)^{-1}. \quad (17)$$

where Θ is the equivalent scattering representation

$$\mathbf{a}_{\text{R}} = \Theta \mathbf{b}_{\text{R}}. \quad (18)$$

The inverse is now given by

$$\mathbf{Z}_{\text{N}}^{-1} = \frac{1}{R} (\mathbf{I} - \Theta)(\mathbf{I} + \Theta)^{-1} \quad (19)$$

and we can write $(\mathbf{I}R + R^2 \mathbf{Z}_{\text{N}}^{-1})$ as

$$\begin{aligned} (\mathbf{I}R + R^2 \mathbf{Z}_{\text{N}}^{-1}) &= \mathbf{I}R + R(\mathbf{I} - \Theta)(\mathbf{I} + \Theta)^{-1} \\ &= R((\mathbf{I} + \Theta) + (\mathbf{I} - \Theta))(\mathbf{I} + \Theta)^{-1} \\ &= 2R(\mathbf{I} + \Theta)^{-1}. \end{aligned} \quad (20)$$

Accordingly, by inserting (20) and (13) into (10), we arrive at the new channel model

$$\begin{aligned} \mathbf{Z}^{\text{DN}} &= \mathbf{Z}_{\text{DS}} - \mathbf{Z}_{\text{DR}}(\mathbf{Z}_{\text{R}} + \mathbf{Z}_{\text{N}}^{\text{DN}})^{-1} \mathbf{Z}_{\text{RS}} \\ &= \mathbf{Z}_{\text{DS}} - R \mathbf{Z}_{\text{DR}} \text{Re}(\mathbf{Z}_{\text{R}})^{-\frac{1}{2}} (\mathbf{I}R + R^2 \mathbf{Z}_{\text{N}}^{-1})^{-1} \text{Re}(\mathbf{Z}_{\text{R}})^{-\frac{1}{2}} \mathbf{Z}_{\text{RS}} \\ &= \mathbf{Z}_{\text{DS}} - R \bar{\mathbf{Z}}_{\text{DR}} (\mathbf{I}R + R^2 \mathbf{Z}_{\text{N}}^{-1})^{-1} \bar{\mathbf{Z}}_{\text{RS}} \\ &= \mathbf{Z}_{\text{DS}} - \frac{1}{2R} \bar{\mathbf{Z}}_{\text{DR}} (\mathbf{I} + \Theta) \bar{\mathbf{Z}}_{\text{RS}} \\ &= \mathbf{Z}_{\text{DS}} + \frac{1}{2R} \bar{\mathbf{Z}}_{\text{DR}} (-\Theta - \mathbf{I}) \bar{\mathbf{Z}}_{\text{RS}} \\ &= \mathbf{Z}_{\text{DS}} + \frac{1}{2R} \bar{\mathbf{Z}}_{\text{DR}} (\bar{\Theta} - \mathbf{I}) \bar{\mathbf{Z}}_{\text{RS}} \end{aligned} \quad (21)$$

with the equivalent scattering matrix

$$\bar{\Theta} = -\Theta. \quad (22)$$

Summarizing the derivations in this section, we arrive at the two equivalent channel representations

$$\begin{aligned} \mathbf{Z}^{\text{DN}} &= \mathbf{Z}_{\text{DS}} - \bar{\mathbf{Z}}_{\text{DR}} (\mathbf{I}R + \bar{\mathbf{Z}}_{\text{N}})^{-1} \bar{\mathbf{Z}}_{\text{RS}} \\ &= \mathbf{Z}_{\text{DS}} + \frac{1}{2R} \bar{\mathbf{Z}}_{\text{DR}} (\bar{\Theta} - \mathbf{I}) \bar{\mathbf{Z}}_{\text{RS}} \end{aligned} \quad (23)$$

which will be analyzed in the following. For both representations in (23) we can notice that the channel model for decoupling networks shares the same structure as a system without mutual coupling between the RIS elements. Hence, all algorithms and solutions, neglecting the mutual coupling of the RIS array, can be extended to mutual coupling by considering the new channel matrices in (15). This is a significant advantage of decoupling networks and we discuss the performance of this approach in Section V.

C. Multiple $\frac{\lambda}{2}$ Spacing

For the special case of a multiple $\frac{\lambda}{2}$ spacing, we have

$$\mathbf{Z}_{\text{R}} = \mathbf{I}R, \quad \text{for } d = \frac{\lambda}{2}k, k \in \mathbb{Z}^+, \quad (24)$$

which results in $\bar{\mathbf{Z}}_{\text{DR}} = \mathbf{Z}_{\text{DR}}$ and $\bar{\mathbf{Z}}_{\text{RS}} = \mathbf{Z}_{\text{RS}}$ and, therefore in the channel model

$$\mathbf{Z}^{\text{DN}} = \mathbf{Z}_{\text{DS}} - \mathbf{Z}_{\text{DR}} (\mathbf{I}R + \bar{\mathbf{Z}}_{\text{N}})^{-1} \mathbf{Z}_{\text{RS}}. \quad (25)$$

We can see that this is exactly the conventional channel model in (1) without mutual coupling. Therefore, for a multiple $\frac{\lambda}{2}$ spacing the decoupled RIS is equal to an uncoupled RIS. It is important that the conventional RIS without decoupling networks is different to the uncoupled RIS even for a multiple $\frac{\lambda}{2}$ spacing as the imaginary part of \mathbf{Z}_{R} is still included in the model which is non-zero for a multiple $\frac{\lambda}{2}$ spacing. Only fully-connected RISs are an exception as they lead to the same model with or without decoupling networks (see Section IV-B for details).

Furthermore, for this special antenna spacing, the implementation of the decoupled RIS can be simplified. The effective impedance network is given by

$$\begin{aligned} \mathbf{Z}_{\text{N}}^{\text{DN}} &= -j\text{Im}(\mathbf{Z}_{\text{R}}) + R \text{Re}(\mathbf{Z}_{\text{R}})^{\frac{1}{2}} \mathbf{Z}_{\text{N}}^{-1} \text{Re}(\mathbf{Z}_{\text{R}})^{\frac{1}{2}} \\ &= -j\text{Im}(\mathbf{Z}_{\text{R}}) + R \mathbf{Z}_{\text{N}}^{-1}. \end{aligned} \quad (26)$$

Therefore, it is possible to omit the decoupling networks and equivalently implement directly the impedance network $\mathbf{Z}_{\text{N}}^{\text{DN}}$. For example, in case of the single-connected RIS, the adjustable impedance network is chosen as

$$\mathbf{Z}_{\text{N}} = -j\text{Im}(\mathbf{Z}_{\text{R}}) - j\text{diag}(\mathbf{x}_{\text{N}}) \quad (27)$$

where the diagonal elements are adjustable. The off-diagonals are static and only depend on the mutual coupling which is the difference to a BD-RIS (see Section IV for details).

IV. CONNECTION TO THE BD-RIS

We have already seen in (12) that independent of \mathbf{Z}_N being diagonal or non-diagonal, the new impedance network \mathbf{Z}_N^{DN} will be generally non-diagonal. Hence, by including a decoupling network into the system model, the resulting network \mathbf{Z}_N^{DN} belongs to the BD-RISs. However, we will see that this is a specific type of BD-RIS which is significantly different from conventional architectures. In this section, we discuss the similarities and the differences of a single-connected RIS with decoupling networks in comparison to a conventional BD-RIS.

A. Diagonal RIS

From (12) we know that the new adjustable impedance network with decoupling networks is given by

$$\mathbf{Z}_N^{\text{DN}} = -j\text{Im}(\mathbf{Z}_R) + R\text{Re}(\mathbf{Z}_R)^{\frac{1}{2}}\mathbf{Z}_N^{-1}\text{Re}(\mathbf{Z}_R)^{\frac{1}{2}} \quad (28)$$

which generally results in a non-diagonal impedance matrix \mathbf{Z}_N^{DN} regardless of the structure of \mathbf{Z}_N . We now assume a diagonal impedance network

$$\mathbf{Z}_N = j\text{diag}(\mathbf{x}_N) \quad (29)$$

for which the new adjustable impedance network \mathbf{Z}_N^{DN} is still non-diagonal. However, the important difference to BD-RISs as they are discussed in the current literature is that the non-diagonal structure of the adjustable impedance network in (28) only results from the mutual coupling. As it only depends on the mutual coupling in the system, the decoupling network is static and independent of the scenario. Hence, the elements of the decoupling networks are not reconfigurable and only have to be calibrated once at the fabrication of the array. Afterwards, the decoupling networks does not change and is valid for any scenario.

This is the difference to the BD-RISs for which the non-diagonal structure is a reconfigurable design parameter that depends on the scenario. In this case, the matrix \mathbf{Z}_N does not only depend on the mutual coupling of the antenna array but is also reconfigured based on the channel realizations or alternatively, its statistics.

It is, however, important to note that decoupling networks and BD-RISs are not competing architectures as they follow inherently different concepts. The decoupling networks are specifically designed for handling the mutual coupling whereas BD-RISs have more degrees of freedom for optimizing the RIS at the cost of an increased complexity. This aspect is independent of whether there exists mutual coupling in the system or not. Specifically, decoupling networks are only designed for the mutual coupling of the RIS array and can be combined with any RIS architecture, including both, the diagonal and BD architectures.

This is further illustrated by the new channel model for decoupling networks according to (23)

$$\mathbf{Z}^{\text{DN}} = \mathbf{Z}_{\text{DS}} + \frac{1}{2R}\bar{\mathbf{Z}}_{\text{DR}}(\bar{\Theta} - \mathbf{I})\bar{\mathbf{Z}}_{\text{RS}}. \quad (30)$$

While the decoupling network has already been applied, the constraint set of $\bar{\Theta}$ (or in the impedance representation

$\bar{\mathbf{Z}}_N$) still plays a major role. Therefore, even when using a decoupling network, the architecture of $\bar{\Theta}$ ($\bar{\mathbf{Z}}_N$) being diagonal or non-diagonal matters. For example, when combining the decoupling network with a diagonal RIS we have the popular unit-modulus constraint set

$$\bar{\Theta} = \text{diag}(\bar{\theta}), \quad |\bar{\theta}_n| = 1 \forall n. \quad (31)$$

Whereas combining the decoupling networks with a fully-connected BD-RIS results in the constraint set

$$\bar{\Theta} = \bar{\Theta}^T \quad \text{and} \quad \bar{\Theta}^H\bar{\Theta} = \mathbf{I}. \quad (32)$$

Additionally, decoupling networks can also be combined with other, partially connected, BD-RIS structures. Please see, e.g., [17] for the different architectures. However, in this article we will only analyze fully-connected and diagonal RISs.

In summary, a decoupling network deals with the mutual coupling of the RIS array and by that it transforms the system model with mutual coupling into a structure that resembles a system model without mutual coupling. However, the decoupling networks can be combined with either a diagonal RIS or a BD-RIS architecture.

B. Fully-Connected BD-RIS

We will now focus on the fully-connected architecture where we can choose an arbitrary impedance matrix

$$\mathbf{Z}_N = j\mathbf{X}_N \quad (33)$$

with the only restriction that it is lossless and reciprocal. As the fully-connected BD-RIS is already capable of implementing any non-diagonal (lossless and reciprocal) impedance matrix, the decoupling networks are not beneficial in this case. When combining the fully-connected tunable network $\mathbf{Z}_N = j\mathbf{X}_N$ with the decoupling network \mathbf{Z}_{DeN} , the effective network according to (12) is given by

$$\mathbf{Z}_N^{\text{DN}} = -j\text{Im}(\mathbf{Z}_R) - jR\text{Re}(\mathbf{Z}_R)^{\frac{1}{2}}\mathbf{X}_N^{-1}\text{Re}(\mathbf{Z}_R)^{\frac{1}{2}}. \quad (34)$$

This network is again lossless and reciprocal as $\text{Re}(\mathbf{Z}_N^{\text{DN}}) = \mathbf{0}$ and $\mathbf{Z}_N^{\text{DN}} = \mathbf{Z}_N^{\text{DN},T}$. As \mathbf{Z}_N^{DN} is a lossless and reciprocal network, there is no advantage of using a decoupling network, as the new network \mathbf{Z}_N^{DN} could be directly implemented with the BD-RIS by choosing

$$\mathbf{Z}_N = -j\text{Im}(\mathbf{Z}_R) + j\frac{1}{R}\text{Re}(\mathbf{Z}_R)^{\frac{1}{2}}\mathbf{X}'_N\text{Re}(\mathbf{Z}_R)^{\frac{1}{2}} \quad (35)$$

where \mathbf{X}'_N is any lossless and reciprocal impedance network. Therefore, for a fully connected RIS a decoupling network is not beneficial and there is a bidirectional mapping between \mathbf{Z}_N^{DN} and \mathbf{Z}_N in (34) and between \mathbf{Z}_N and \mathbf{X}'_N in (35).

It is indeed quite intuitive that the decoupling network is unnecessary for a fully-connected BD-RIS. Since we can anyway design an arbitrary lossless reciprocal network when incorporating a fully-connected BD-RIS, connecting a second lossless reciprocal network does not give us more design choices. While the decoupling networks provide no benefits in this case, it can still be exploited that their special structure leads to a channel decomposition corresponding to having no

mutual coupling. Using (35), the equivalent channel for the BD-RIS can be written as

$$\mathbf{Z} = \mathbf{Z}_{\text{DS}} - \bar{\mathbf{Z}}_{\text{DR}}(\mathbf{I}\mathbf{R} + \mathbf{j}\mathbf{X}'_{\text{N}})^{-1}\bar{\mathbf{Z}}_{\text{RS}} \quad (36)$$

which follows the exact same structure when having no mutual coupling and is a direct consequence when utilizing decoupling networks. Hence, when using a fully-connected BD-RIS, the decompositions in (34)–(36) introduced in [1] are also present when having no decoupling network [31].

V. CHANNEL AND ARRAY GAIN MAXIMIZATION

We have already seen that decoupling networks result in a channel model which has the same structure as a system without mutual coupling. In this section, we analyze the resulting performance of the decoupling networks in comparison to a conventional RIS with mutual coupling but without the decoupling networks. Moreover, in this section, we also provide an analytic discussion on the influence of mutual coupling on RIS-aided systems. Specifically we consider the channel and array gain of a single-user SISO system. Hence, the BS is assumed to have one antenna serving a single user with also one antenna. The RIS, however, can have an arbitrary number of RIS elements N . The channel model for this scenario, when using decoupling networks, reads according to (23) as

$$z^{\text{DN}} = z_{\text{DS}} + \frac{1}{2R}\bar{\mathbf{z}}_{\text{DR}}^{\text{T}}(\bar{\Theta} - \mathbf{I})\bar{\mathbf{z}}_{\text{RS}} \quad (37)$$

where the matrix $\bar{\Theta}$ can be either diagonal or non-diagonal depending on the RIS architecture. As (37) has the structure of a system without mutual coupling, the maximization of $|z^{\text{DN}}|^2$ can be given in closed-form and in case of a diagonal RIS $\bar{\Theta} = \text{diag}(\bar{\theta})$, the optimal solution reads as [27]

$$\bar{\theta} = \exp\left(\mathbf{j} \arg\left(z_{\text{DS}} - \frac{1}{2R}\bar{\mathbf{z}}_{\text{DR}}^{\text{T}}\bar{\mathbf{z}}_{\text{RS}}\right) \mathbf{1} - \mathbf{j} \arg(\bar{\mathbf{z}}_{\text{DR}} \odot \bar{\mathbf{z}}_{\text{RS}})\right) \quad (38)$$

with the corresponding channel gain given by

$$|z_{\text{D}}^{\text{DN}}|^2 = \left(\left| z_{\text{DS}} - \frac{1}{2R}\bar{\mathbf{z}}_{\text{DR}}^{\text{T}}\bar{\mathbf{z}}_{\text{RS}} \right| + \frac{1}{2R} \sum_{n=1}^N |\bar{z}_{\text{DR},n}| |\bar{z}_{\text{RS},n}| \right)^2. \quad (39)$$

For the fully-connected BD-RIS, on the other hand, we use an upper bound (see [17]) for which the channel gain is given by

$$|z_{\text{BD}}^{\text{DN}}|^2 \leq \left(\left| \bar{z}_{\text{DS}} - \frac{1}{2R}\bar{\mathbf{z}}_{\text{DR}}^{\text{T}}\bar{\mathbf{z}}_{\text{RS}} \right| + \frac{1}{2R} \|\bar{\mathbf{z}}_{\text{DR}}\|_2 \|\bar{\mathbf{z}}_{\text{RS}}\|_2 \right)^2. \quad (40)$$

Interestingly, in [18], it has been shown that this upper bound can be achieved with the fully-connected BD-RIS and, hence, (40) is the actual channel gain of the BD-RIS. Throughout this section we assume the BD-RIS to be always fully-connected. As the BD-RIS has more degrees of freedom we can already see that

$$|z_{\text{D}}^{\text{DN}}|^2 \leq |z_{\text{BD}}^{\text{DN}}|^2 \quad (41)$$

holds and the BD-RIS leads, therefore, in general to a better performance.

A. Scenario

To analyze the channel/array gain for the different architectures, we assume a line of sight (LOS) scenario according to Fig. 2 where the direct channel from the BS to the user is blocked, i.e., $z_{\text{DS}} = 0 \Omega$.

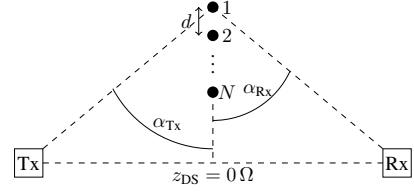


Fig. 2. SISO Link with N Elements at the RIS.

We assume a uniform linear array (ULA) at the RIS which results in the channels

$$z_{\text{DS}} = 0 \Omega, \quad z_{\text{DR}}^{\text{T}} = \sqrt{\gamma_{\text{DR}}}\mathbf{a}_{\text{DR}}^{\text{T}}R, \quad z_{\text{RS}} = \sqrt{\gamma_{\text{RS}}}\mathbf{a}_{\text{RS}}R \quad (42)$$

where $\sqrt{\gamma_{\text{DR}}}$, $\sqrt{\gamma_{\text{RS}}}$ are the pathlosses and $\mathbf{a}_{\text{DR}} = \mathbf{a}(\alpha_{\text{RX}})$, $\mathbf{a}_{\text{RS}} = \mathbf{a}(\alpha_{\text{TX}})$ the LOS ULA vectors where the n -th entry $a_n(\alpha)$ is given by

$$a_n(\alpha) = e^{-\mathbf{j}(n-1)2\pi\frac{d}{\lambda}\cos(\alpha)}. \quad (43)$$

The channel gain for one RIS element ($N = 1$), reads for both, the diagonal and the BD-RIS as $|z^{\text{DN}}|^2 = \gamma_{\text{DR}}\gamma_{\text{RS}}R^2$. Normalizing the channel gain for N elements by the gain of one element, we arrive at the array gain

$$A_{\text{D}}^{\text{DN}} = \frac{1}{4} \left(\left| \mathbf{a}_{\text{DR}}^{\text{T}}\mathbf{C}_{\text{R}}^{-1}\mathbf{a}_{\text{RS}} \right| + \sum_{n=1}^N \left| \mathbf{a}_{\text{DR}}^{\text{T}}\mathbf{C}_{\text{R}}^{-\frac{1}{2}}\mathbf{e}_n \right| \left| \mathbf{e}_n^{\text{T}}\mathbf{C}_{\text{R}}^{-\frac{1}{2}}\mathbf{a}_{\text{RS}} \right| \right)^2 \quad (44)$$

for the diagonal RIS and at

$$A_{\text{BD}}^{\text{DN}} = \frac{1}{4} \left(\left| \mathbf{a}_{\text{DR}}^{\text{T}}\mathbf{C}_{\text{R}}^{-1}\mathbf{a}_{\text{RS}} \right| + \sqrt{\mathbf{a}_{\text{DR}}^{\text{H}}\mathbf{C}_{\text{R}}^{-1}\mathbf{a}_{\text{DR}}\mathbf{a}_{\text{RS}}^{\text{H}}\mathbf{C}_{\text{R}}^{-1}\mathbf{a}_{\text{RS}}} \right)^2 \quad (45)$$

for the BD-RIS where we used the definition

$$\mathbf{C}_{\text{R}} = \frac{1}{R}\text{Re}(\mathbf{Z}_{\text{R}}). \quad (46)$$

It of course still holds that

$$A_{\text{D}}^{\text{DN}} \leq A_{\text{BD}}^{\text{DN}}. \quad (47)$$

Additionally, we know that the fully-connected BD-RIS without a decoupling network is equivalent to a fully-connected BD-RIS with a decoupling network. Hence, we also have

$$A_{\text{BD}}^{\text{DN}} = A_{\text{BD}} \quad (48)$$

where A_{BD} is the array gain of a conventional system without the decoupling network. Thus, $A_{\text{BD}}^{\text{DN}}$ and A_{BD} can be used interchangeably.

First, we compare the BD-RIS and the diagonal RIS structure for the setup $\alpha_{\text{TX}} = 0$, $\alpha_{\text{RX}} = \frac{\pi}{2}$ in Fig. 3. Interestingly, for small element spacings the diagonal RIS (dashed curves) with $2k-1$ elements performs better performance than with $2k$

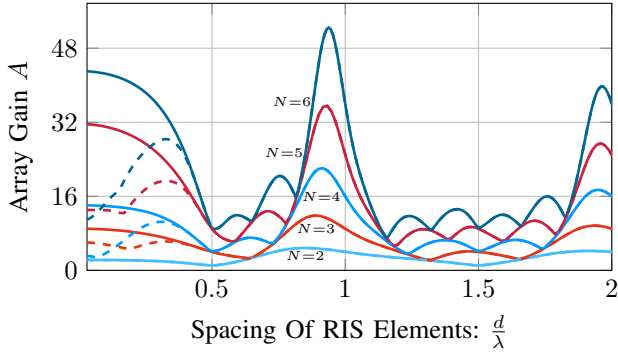


Fig. 3. Array Gain for $\alpha_{\text{Tx}} = 0$ and $\alpha_{\text{Rx}} = \frac{\pi}{2}$. The BD-RIS has solid curves and the diagonal RIS has dashed curves.

elements. For the BD-RIS (solid curves), this is different and increasing the number of elements monotonically improves the performance for any spacing. Additionally, we can observe that for small element spacings, the BD-RIS leads to a better performance in comparison to the diagonal RIS, whereas for an increased spacing $d \geq \frac{\lambda}{2}$ there is no difference between the two architectures. Hence, we will further study the transition point $d = \frac{\lambda}{2}$ in the following.

B. Multiple $\frac{\lambda}{2}$ spacing

In the case of having an element spacing of

$$d = \frac{\lambda}{2}k, k \in \mathbb{Z}^+, \quad (49)$$

the matrix \mathbf{C}_R results in the identity matrix, i.e.,

$$\mathbf{C}_R = \mathbf{I}. \quad (50)$$

From Section III-C we know that in this case a decoupled RIS is equal to an uncoupled RIS whereas the conventional RIS without decoupling networks leads to a different model. Only the fully-connected BD-RIS is an exception as the system model is identical with or without decoupling networks (see Section IV-B). We are comparing the performance of the various architectures in case of a multiple $\frac{\lambda}{2}$ spacing. The channel gain of a diagonal RIS with decoupling networks is given as

$$\begin{aligned} A_D^{\text{DN}} &= \frac{1}{4} \left(|\mathbf{a}_{\text{DR}}^{\text{T}} \mathbf{a}_{\text{RS}}| + \sum_{n=1}^N |\mathbf{a}_{\text{DR}}^{\text{T}} \mathbf{e}_n| |e_n^{\text{T}} \mathbf{a}_{\text{RS}}| \right)^2 \\ &= \frac{1}{4} (|\mathbf{a}_{\text{DR}}^{\text{T}} \mathbf{a}_{\text{RS}}| + N)^2. \end{aligned} \quad (51)$$

Additionally, for the BD-RIS we arrive at the channel gain

$$\begin{aligned} A_{\text{BD}} &= A_{\text{BD}}^{\text{DN}} = \frac{1}{4} \left(|\mathbf{a}_{\text{DR}}^{\text{T}} \mathbf{a}_{\text{RS}}| + \sqrt{\mathbf{a}_{\text{DR}}^{\text{H}} \mathbf{a}_{\text{DR}} \mathbf{a}_{\text{RS}}^{\text{H}} \mathbf{a}_{\text{RS}}} \right)^2 \\ &= \frac{1}{4} (|\mathbf{a}_{\text{DR}}^{\text{T}} \mathbf{a}_{\text{RS}}| + N)^2 \\ &= A_D^{\text{DN}} \end{aligned} \quad (52)$$

where $A_{\text{BD}} = A_{\text{BD}}^{\text{DN}}$ is given in (48). Therefore, the BD-RIS and the diagonal RIS have the same performance

$$A_{\text{BD}} = A_{\text{BD}}^{\text{DN}} = A_D^{\text{DN}} \quad (53)$$

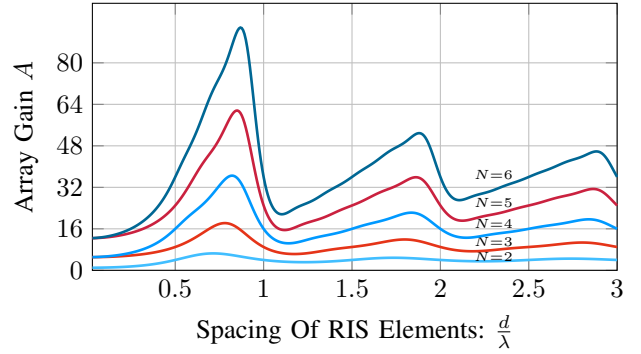


Fig. 4. Array Gain for the front-fire direction of the array.

for a multiple $\frac{\lambda}{2}$ spacing and are equal to an uncoupled RIS array. With these comparisons it is also possible to compare the conventional diagonal RIS with the decoupled RIS. The decoupled RIS leads for this spacing always to a better performance as

$$A_D^{\text{DN}} = A_{\text{BD}} \geq A_D \quad (54)$$

where A_D is the array gain of the conventional diagonal RIS. This also means that at $d = \frac{\lambda}{2}$ an uncoupled diagonal RIS will always perform better in comparison to a diagonal RIS with mutual coupling.

C. Specular Reflection Scenario

We now return to an arbitrary spacing d . In particular, the specular reflection scenario is now investigated, where we have

$$\alpha_{\text{Tx}} = \pi - \alpha_{\text{Rx}}, \quad \text{and, hence,} \quad \mathbf{a}_{\text{DR}} = \mathbf{a}_{\text{RS}}^*. \quad (55)$$

Two particular important scenarios, the front-fire and the end-fire direction belong to this specular type and are investigated below in detail. For the specular case, the array gain of the diagonal RIS is given as

$$\begin{aligned} A_D^{\text{DN}} &= \frac{1}{4} \left(|\mathbf{a}_{\text{DR}}^{\text{T}} \mathbf{C}_R^{-1} \mathbf{a}_{\text{RS}}| + \sum_{n=1}^N |\mathbf{a}_{\text{DR}}^{\text{T}} \mathbf{C}_R^{-\frac{1}{2}} \mathbf{e}_n| |e_n^{\text{T}} \mathbf{C}_R^{-\frac{1}{2}} \mathbf{a}_{\text{RS}}| \right)^2 \\ &= \frac{1}{4} \left(\mathbf{a}_{\text{RS}}^{\text{H}} \mathbf{C}_R^{-1} \mathbf{a}_{\text{RS}} + \sum_{n=1}^N |\mathbf{a}_{\text{RS}}^{\text{H}} \mathbf{C}_R^{-\frac{1}{2}} \mathbf{e}_n| |e_n^{\text{T}} \mathbf{C}_R^{-\frac{1}{2}} \mathbf{a}_{\text{RS}}| \right)^2 \\ &= \frac{1}{4} \left(\mathbf{a}_{\text{RS}}^{\text{H}} \mathbf{C}_R^{-1} \mathbf{a}_{\text{RS}} + \left\| \mathbf{C}_R^{-\frac{1}{2}} \mathbf{a}_{\text{RS}} \right\|^2 \right)^2 \\ &= (\mathbf{a}_{\text{RS}}^{\text{H}} \mathbf{C}_R^{-1} \mathbf{a}_{\text{RS}})^2 \end{aligned} \quad (56)$$

whereas the array gain of the BD-RIS is given by

$$\begin{aligned} A_{\text{BD}} &= \frac{1}{4} \left(|\mathbf{a}_{\text{DR}}^{\text{T}} \mathbf{C}_R^{-1} \mathbf{a}_{\text{RS}}| + \sqrt{\mathbf{a}_{\text{DR}}^{\text{H}} \mathbf{C}_R^{-1} \mathbf{a}_{\text{DR}} \mathbf{a}_{\text{RS}}^{\text{H}} \mathbf{C}_R^{-1} \mathbf{a}_{\text{RS}}} \right)^2 \\ &= \frac{1}{4} (\mathbf{a}_{\text{RS}}^{\text{H}} \mathbf{C}_R^{-1} \mathbf{a}_{\text{RS}} + \mathbf{a}_{\text{RS}}^{\text{H}} \mathbf{C}_R^{-1} \mathbf{a}_{\text{RS}})^2 \\ &= (\mathbf{a}_{\text{RS}}^{\text{H}} \mathbf{C}_R^{-1} \mathbf{a}_{\text{RS}})^2. \end{aligned} \quad (57)$$

Hence, the BD-RIS and the diagonal RIS lead to the same performance

$$A_D^{\text{DN}} = A_{\text{BD}} = (\mathbf{a}_{\text{RS}}^{\text{H}} \mathbf{C}_R^{-1} \mathbf{a}_{\text{RS}})^2. \quad (58)$$

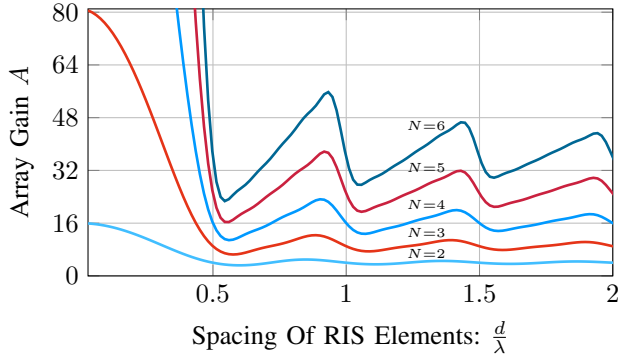


Fig. 5. Array Gain for the end-fire direction of the array.

Interestingly, this is exactly the square of a conventional transmit array gain at the BS (see [22] for the transmit array gain). From (58) it also directly follows that

$$A_D^{\text{DN}} = A_{\text{BD}} \geq A_D \quad (59)$$

and, hence, the diagonal RIS with decoupling network always outperforms the conventional diagonal RIS in this specular reflection scenario. Two particular scenarios are now further investigated, the front-fire as well as the end-fire directions.

Front-Fire: In the case of having impinging waves in the front-fire direction we have $\alpha_{\text{Rx}} = \alpha_{\text{Tx}} = \frac{\pi}{2}$ and, hence, $\mathbf{a}_{\text{RS}} = \mathbf{a}_{\text{DR}} = \mathbf{1}$. The array gain, therefore, reads as

$$A_D^{\text{DN}} = A_{\text{BD}} = (\mathbf{1}^T \mathbf{C}_R^{-1} \mathbf{1})^2 \quad (60)$$

and we arrive at Fig. 4. In fact, the array gains in Fig. 4 correspond to the ones in [22, Fig. 6] with the key difference of having squared values. We also notice that for $2k$ and for $2k - 1$ elements the array gain converges to the same value for $d \rightarrow 0$. Please note, that the BD-RIS and the diagonal RIS lead to the same performance in this scenario.

End-Fire: In case of the end-fire direction we have $\alpha_{\text{Rx}} = \pi$, $\alpha_{\text{Tx}} = 0$ and, hence, $\mathbf{a}_{\text{RS}} = \mathbf{a}_0$, $\mathbf{a}_{\text{DR}} = \mathbf{a}_0^*$ with $\mathbf{a}_0 = \mathbf{a}(0)$. Therefore, we arrive at the array gain

$$A_D^{\text{DN}} = A_{\text{BD}} = (\mathbf{a}_0^H \mathbf{C}_R^{-1} \mathbf{a}_0)^2 \quad (61)$$

which is illustrated in Fig. 5. Here, the gains correspond to those in [22, Fig. 5] with squared values and we also observe a significant gain for $d \rightarrow 0$ as in [22]. By utilizing [32]

$$\lim_{d \rightarrow 0} \mathbf{a}_0^H \mathbf{C}_R^{-1} \mathbf{a}_0 = N^2 \quad (62)$$

we obtain a quartic array gain in case of having a RIS in end-fire direction, i.e.,

$$\lim_{d \rightarrow 0} A_D^{\text{DN}} = \lim_{d \rightarrow 0} A_{\text{BD}} = \lim_{d \rightarrow 0} (\mathbf{a}_0^H \mathbf{C}_R^{-1} \mathbf{a}_0)^2 = N^4. \quad (63)$$

Hence, we can directly conclude that a super-quadratic array gain is possible when implementing a RIS in the end-fire direction. Note again that in this case the BD-RIS and the diagonal RIS lead to the same performance according to (58). This super-quadratic gain clearly exceeds the gain of N^2 which has been generally assumed in existing literature.

The question arises whether this super-quadratic gain can be generalized to more cases except of being in end-fire direction and we will analyze this in the following.

VI. SUPER-QUADRATIC GAIN

We have seen that, specifically for the end-fire direction, a super-quadratic gain of

$$\lim_{d \rightarrow 0} (\mathbf{a}_0^H \mathbf{C}_R^{-1} \mathbf{a}_0)^2 = N^4 \quad (64)$$

is possible for both the diagonal RIS as well as the BD-RIS. In this section, we further investigate and generalize our result in (64).

A. Maximum at End-Fire

Firstly, it is important to note that the end-fire direction gives the maximum possible gain in a RIS-assisted scenario for $d \rightarrow 0$ which we summarize in the following theorem.

Theorem 1. *The maximum array gain of a decoupled RIS for $d \rightarrow 0$ is given by*

$$\lim_{d \rightarrow 0} A_{\text{D/BD}}^{\text{DN}} \leq (\lim_{d \rightarrow 0} \mathbf{a}_0^H \mathbf{C}_R^{-1} \mathbf{a}_0)^2 = N^4 \quad (65)$$

which is achievable for both the BD as well as the diagonal RIS with decoupling networks. Additionally, it follows that

$$A_D^{\text{DN}} = A_{\text{BD}} \geq A_D \quad (66)$$

and, hence, the conventional RIS without decoupling networks cannot exceed this gain.

Proof. We start with the array gain of the BD-RIS (45)

$$\begin{aligned} |\mathbf{a}_{\text{DR}}^T \mathbf{C}_R^{-1} \mathbf{a}_{\text{RS}}| &= \left| \mathbf{a}_{\text{DR}}^T \mathbf{C}_R^{-\frac{1}{2}} \mathbf{C}_R^{-\frac{1}{2}} \mathbf{a}_{\text{RS}} \right| \\ &\leq \left\| \mathbf{a}_{\text{DR}}^T \mathbf{C}_R^{-\frac{1}{2}} \right\|_2 \left\| \mathbf{C}_R^{-\frac{1}{2}} \mathbf{a}_{\text{RS}} \right\|_2 \\ &= \sqrt{\mathbf{a}_{\text{DR}}^H \mathbf{C}_R^{-1} \mathbf{a}_{\text{DR}} \mathbf{a}_{\text{RS}}^H \mathbf{C}_R^{-1} \mathbf{a}_{\text{RS}}} \end{aligned} \quad (67)$$

and, hence, we can bound the gain of the BD-RIS as

$$\begin{aligned} A_{\text{BD}} &= \frac{1}{4} \left(|\mathbf{a}_{\text{DR}}^T \mathbf{C}_R^{-1} \mathbf{a}_{\text{RS}}| + \sqrt{\mathbf{a}_{\text{DR}}^H \mathbf{C}_R^{-1} \mathbf{a}_{\text{DR}} \mathbf{a}_{\text{RS}}^H \mathbf{C}_R^{-1} \mathbf{a}_{\text{RS}}} \right)^2 \\ &\leq \mathbf{a}_{\text{DR}}^H \mathbf{C}_R^{-1} \mathbf{a}_{\text{DR}} \mathbf{a}_{\text{RS}}^H \mathbf{C}_R^{-1} \mathbf{a}_{\text{RS}}. \end{aligned} \quad (68)$$

From the analysis of the transmit array [32] we know that

$$\lim_{d \rightarrow 0} \mathbf{a}_{\text{RS}}^H \mathbf{C}_R^{-1} \mathbf{a}_{\text{RS}} \leq \lim_{d \rightarrow 0} \mathbf{a}_0^H \mathbf{C}_R^{-1} \mathbf{a}_0 = N^2 \quad (69)$$

and, hence, the end-fire direction gives the largest gain for $d \rightarrow 0$. Therefore, we arrive at

$$\lim_{d \rightarrow 0} A_{\text{BD}} \leq (\lim_{d \rightarrow 0} \mathbf{a}_0^H \mathbf{C}_R^{-1} \mathbf{a}_0)^2 = N^4. \quad (70)$$

This upper bound for $d \rightarrow 0$ is achievable in the end-fire direction. It is important to note that this maximum gain is also achievable by the diagonal RIS in the end-fire direction

$$\lim_{d \rightarrow 0} A_D^{\text{DN}} = (\lim_{d \rightarrow 0} \mathbf{a}_0^H \mathbf{C}_R^{-1} \mathbf{a}_0)^2 = N^4 \quad (71)$$

and, hence, the BD-RIS and the diagonal RIS have the same maximum channel gain which is quartic. \square

B. Super-Quadratic Gain of Coupled RISs

From the last sections we know that the gain of an uncoupled RIS/decoupled RIS at $\frac{\lambda}{2}$ is given by

$$A_{BD} = A_D^{DN} = \frac{1}{4} (|\mathbf{a}_{DR}^T \mathbf{a}_{RS}| + N)^2 \leq N^2 \quad (72)$$

whereas for the coupled RIS for $d \rightarrow 0$ it is given by

$$A_{BD} = A_D^{DN} = N^4. \quad (73)$$

This shows that mutual coupling can lead to a significantly better performance in comparison to an uncoupled RIS array (decoupled RIS array with $d = \frac{\lambda}{2}$). However, the requirement of using (62) for deriving Theorem 1 indicates that the quartic gain is only achievable in the case of placing the BS, the RIS as well as the user exactly in end-fire direction. Indeed, similar to the case for transmit arrays in [22], when placing them in front-fire direction, mutual coupling for $d \rightarrow 0$ decreases the gain compared to having no mutual coupling (cf. Fig 4). However, there is a major difference in comparison to a conventional transmit array. While we cannot know the position of the user and, hence, cannot ensure to be in end-fire direction, it is possible to position the RIS and the BS as desired.

Hence, it is possible to place the RIS and the BS in end-fire direction illustrated in Fig. 6. We already know that if the

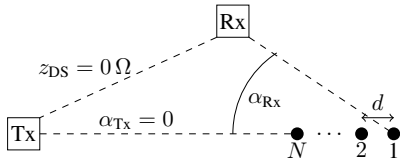


Fig. 6. BS and RIS positioned in end-fire direction.

user is in the end-fire direction, i.e., $\alpha_{Rx} = \pi$, we observe a super-quadratic gain of N^4 for $d \rightarrow 0$, significantly exceeding the N^2 gain of an uncoupled RIS (or decoupled RIS with $\frac{\lambda}{2}$ spacing). For other user angles α_{Rx} this is not the case. However, we will show that it is still possible for the BD-RIS to achieve a super-quadratic gain in the order of N^3 . Since we position the BS and the RIS in end-fire direction, we obtain the array gain (cf. (45))

$$\begin{aligned} A_{BD} &= \frac{1}{4} \left(|\mathbf{a}_{DR}^T \mathbf{C}_R^{-1} \mathbf{a}_0| + \sqrt{\mathbf{a}_{DR}^H \mathbf{C}_R^{-1} \mathbf{a}_{DR} \mathbf{a}_0^H \mathbf{C}_R^{-1} \mathbf{a}_0} \right)^2 \\ &\geq \frac{1}{4} \mathbf{a}_{DR}^H \mathbf{C}_R^{-1} \mathbf{a}_{DR} \mathbf{a}_0^H \mathbf{C}_R^{-1} \mathbf{a}_0. \end{aligned} \quad (74)$$

Hence, for $d \rightarrow 0$, we can again utilize (62) and observe that the array gain still exhibits a lower bound, i.e.,

$$\lim_{d \rightarrow 0} A_{BD} \geq \frac{N^2}{4} \lim_{d \rightarrow 0} \mathbf{a}_{DR}^H \mathbf{C}_R^{-1} \mathbf{a}_{DR}. \quad (75)$$

In consequence, placing the BS and the RIS in end-fire direction leads to an N^2 scaling for small antenna spacings. However, the lower bound in (75) also contains the term $\mathbf{a}_{DR}^H \mathbf{C}_R^{-1} \mathbf{a}_{DR}$ which is the expression of a conventional

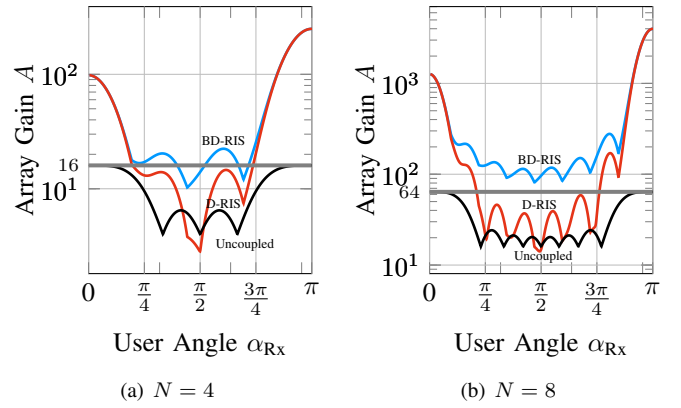


Fig. 7. Array Gain over the user angle for $d = \frac{\lambda}{32}$.

transmit array gain and depends on the user angle α_{Rx} . This expression is analyzed in the following. From [32] we know that the conventional array gain for a coupled array reads as

$$\lim_{d \rightarrow 0} \mathbf{a}_{DR}^H \mathbf{C}_R^{-1} \mathbf{a}_{DR} = \sum_{n=0}^{N-1} (2n+1) P_n^2(\cos(\alpha_{Rx})) \quad (76)$$

where $P_n(x)$ is the Legendre polynomial of degree n . To end up with a super-quadratic lower bound on the array gain in (75), we start with the following proposition

Proposition 1. *The function $f_N(x) = \sum_{n=0}^{N-1} (2n+1) P_n^2(x)$ with $x \in [-1, 1]$ is lower bounded by*

$$f_N(x) \geq \frac{N}{2} \quad \forall x \quad (77)$$

and its global minimum is given by $f(x_{min}) = N^2 P_N^2(x_{min})$. For even N the global minimum is attained at $x_{min} = 0$, whereas for odd N the global minima are at $x_{min} = \pm x_0$ where x_0 is the positive zero of the derivative $P'_N(x)$ which is closest to $x = 0$.

Proof. Please see Appendix A. \square

Corollary 1. *The conventional transmit antenna gain $\mathbf{a}_{DR}^H \mathbf{C}_R^{-1} \mathbf{a}_{DR}$ for $d \rightarrow 0$ attains its minimum gain in the front-fire direction ($\alpha_{Rx} = \frac{\pi}{2}$) for even N . Additionally, the antenna gain is bounded by*

$$\lim_{d \rightarrow 0} \mathbf{a}_{DR}^H \mathbf{C}_R^{-1} \mathbf{a}_{DR} \geq \frac{N}{2}. \quad (78)$$

Proof. This follows directly from Proposition 1 and (76). \square

It should be noted that Corollary 1 also holds for the conventional transmit array gain when no RIS is employed in the system. By combining Corollary 1 and (75), we derive the following theorem.

Theorem 2. *The array gain of a BD-RIS for $d \rightarrow 0$ achieves a super-quadratic gain of at least*

$$\lim_{d \rightarrow 0} A_{BD} \geq \frac{N^3}{8}. \quad (79)$$

This holds for any user angle α_{Rx} .

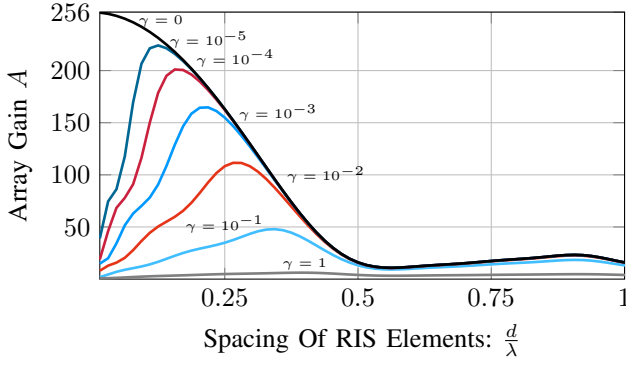


Fig. 8. Array Gain for the end-fire direction of the array for $N = 4$.

By comparing the upper bound on the array gain of an uncoupled RIS in (72) with the lower bound on the array gain of BD-RISs in Theorem 2, we observe that for $N \geq 8$ the coupled RIS outperforms the uncoupled one when $d \rightarrow 0$ and considering no other losses. More importantly, the coupled RIS scales super-quadratic with the number of RIS elements as N^3 in comparison to an uncoupled RIS which only scales with N^2 . Theorem 2 is illustrated in Fig. 7. We can see that for both $N = 4$ as well as for $N = 8$ the BD-RIS leads to a better performance in comparison to the diagonal RIS. Only for the end-fire direction they achieve the same performance which validates our theoretical result in Theorem 1. Moreover, Fig. 7 also validates Theorem 2. For $N = 4$, the BD-RIS achieves a good performance but it does not exceed N^2 for all user angles which is the maximum gain of the uncoupled RIS. This is different to $N = 8$, where we can see that regardless of the user, the BD-RIS leads to a better performance.

C. Ohmic Losses

We have seen in the last section that the coupled RIS leads to significant improvements in comparison to an uncoupled RIS, achieving an N^4 gain in the end-fire direction. Moreover, the BD-RIS leads to at least a cubic gain for all user angles. However, we considered lossless antenna arrays where the spacing $d \rightarrow 0$ and the simulations are based on a very small spacing of $d = \frac{\lambda}{32}$. We will now investigate these super-quadratic gains under more realistic circumstances. Equivalent to [22] we assume Ohmic losses and when including the dissipation resistance of R_d , we obtain the new coupling matrix

$$\mathbf{Z}_R^{\text{loss}} = \mathbf{Z}_R + \mathbf{I}R_d. \quad (80)$$

The real part of \mathbf{Z}_R with the values R on the diagonal is now combined with the resistance R_d . Similarly, we obtain

$$\mathbf{C}_R^{\text{loss}} = \mathbf{Z}_R^{\text{loss}} \frac{1}{R} = \mathbf{C}_R + \gamma \mathbf{I} \quad (81)$$

with $\gamma = \frac{R_d}{R}$ and R_d being the dissipation resistance. Hence, the ideal coupling matrix \mathbf{C}_R is now regularized by $\gamma \mathbf{I}$. We first study the end-fire direction where the largest (the N^4 gain)

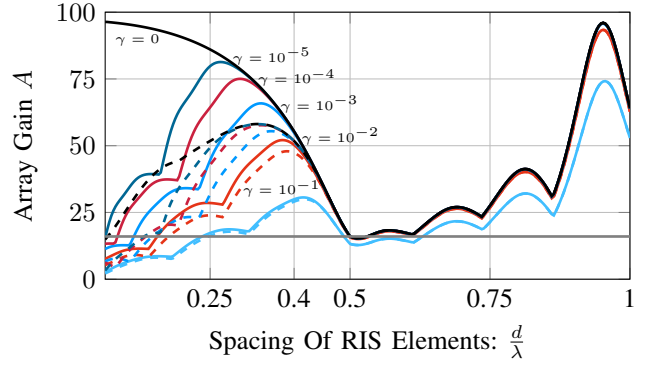


Fig. 9. Array Gain for the $\alpha_{\text{Tx}} = 0$ and $\alpha_{\text{Rx}} = \frac{\pi}{2}$ and $N = 8$. The BD-RIS has solid curves and the diagonal RIS has dashed curves.

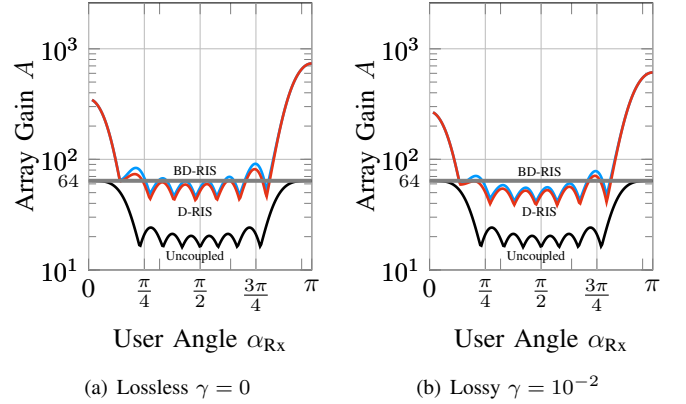


Fig. 10. Array Gain over the user angle for $d = 0.4$ and $N = 8$.

appears for the ideal lossless array. Including Ohmic losses we arrive at the new expression

$$A_D^{\text{DN}} = A_{\text{BD}} = (\mathbf{a}_0^H (\mathbf{C}_R + \gamma \mathbf{I})^{-1} \mathbf{a}_0)^2 \quad (82)$$

for the end-fire direction, where we can observe that the array gain decreases with an increasing γ . Additionally, the higher the value of γ , the stronger the diagonal loading of the matrix $(\mathbf{C}_R + \gamma \mathbf{I})$ and, hence, the more similar the scenario to the case without mutual coupling.

The resulting performance when considering Ohmic losses is illustrated in Fig. 8 and resembles [22, Fig. 11] with squared values.

We observe that a very small element spacing actually leads to a large degradation in the performance when considering Ohmic losses in the array. Furthermore, the optimal spacing of the elements increases for increasing losses. This behavior can also be observed for $\alpha_{\text{Tx}} = 0$ and $\alpha_{\text{Rx}} = \frac{\pi}{2}$ in Fig. 9 where an increased spacing is necessary when losses are considered in the model. The lossless curves in Fig. 9 (see also Fig. 3) show a significant difference between the BD-RIS and the diagonal RIS for small spacings. However, as the spacing increases, the difference between the two architectures decreases and eventually vanishes. When including losses, an increased spacing is necessary and we can see that the

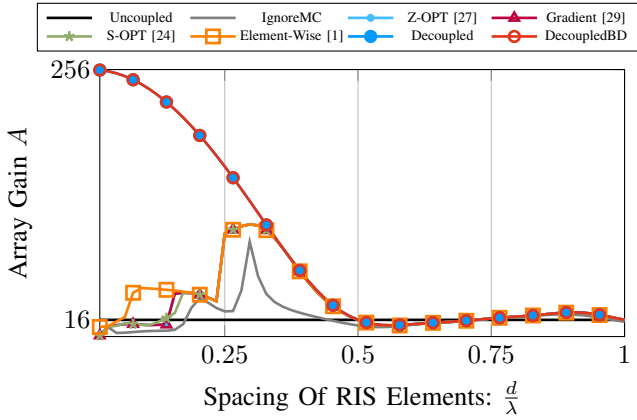


Fig. 11. End-Fire direction for $N = 4$.

difference between the BD-RIS and the diagonal RIS decrease for increasing losses.

This is further investigated in Fig. 10 for $\gamma = 10^{-2}$ and a spacing of $d = 0.4$ (see Fig. 9). In the lossless case, we can see that the increased spacing deteriorates the performance of the BD-RIS and increases the performance of the diagonal RIS. This is in accordance with Fig. 3 and the lossless curve of Fig. 9. Hence, for this more practical spacing, the advantage of the BD-RIS over the diagonal RIS is almost neglectable and they lead to roughly the same performance. When including losses, the performance is very similar to the lossless case which is the advantage of choosing the spacing $d = 0.4\lambda$. In this case, the super-quadratic cannot be ensured anymore, but can still be observed around $\alpha_{R_x} = 0$ and $\alpha_{R_x} = \pi$.

VII. NUMERICAL RESULTS

In this section, we evaluate the decoupling network together with the mutual coupling aware algorithms in the same LOS scenario as in Section V according to Fig. 2. We focus on the diagonal RIS where we compare the proposed decoupling network (Decoupled) with various algorithms for the conventional RIS array under mutual coupling. This includes the element-wise approach discussed in [1] (Element-Wise) together with the gradient approach of [29] (Gradient), the Neumann series approach of [27] (Z-OPT), and the two scattering parameter-based approaches in [24] (S-UNI and S-OPT). As in [24], S-OPT leads to better results than S-UNI in our analysis and, hence, S-UNI is omitted in the comparison. To further evaluate the results, we include a RIS array without mutual coupling (Uncoupled) where we set $\mathbf{Z}_R = \mathbf{I}R$. This is equal to a decoupled RIS with a multiple $\frac{\lambda}{2}$ spacing. Additionally, we include a naive optimization (IgnoreMC) where we solve the channel maximization by ignoring mutual coupling (assuming $\mathbf{Z}_R = \mathbf{I}R$) but then use the actual model with the non-diagonal coupling matrix \mathbf{Z}_R for the evaluation. All the methods above are also initialized by this solution, i.e., by first ignoring the mutual coupling. Please note that all baselines, i.e., Element-Wise, Gradient, Z-OPT, S-UNI and S-OPT require an iterative optimization whereas our proposed

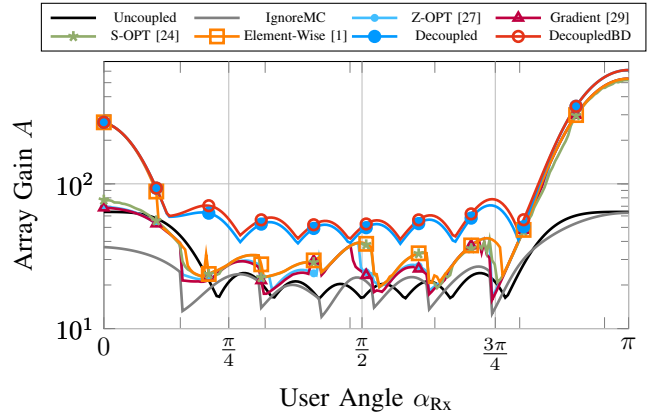


Fig. 12. Element spacing of $d = 0.4\lambda$ including losses with $\gamma = 10^{-2}$ for $N = 8$.

Decoupled enables closed-form solutions. Additionally, we evaluate also the fully-connected BD-RIS as an upper bound. Please note that according to Section IV-B, the fully-connected RIS has the same performance with or without decoupling networks. Hence, DecoupledBD is the performance for both versions. In all simulations we consider the array gain as our metric.

First, we compare all methods for the end-fire direction with $N = 4$ elements in Fig. 11. Here, the quartic gain is achievable for $d \rightarrow 0$. Since, additionally, the matrix $\text{Re}(\mathbf{Z}_R)$ becomes ill-conditioned for $d \rightarrow 0$, small spacings are computationally challenging. For this scenario, the uncoupled method is significantly worse than the methods including mutual coupling and it is only well performing for $d \geq \frac{\lambda}{2}$. The decoupling networks, on the other hand, lead to a quartic gain according to Theorem 1 and, additionally, Decoupled has the same performance as DecoupledBD (see Theorem 1). Moreover, the decoupling networks are clearly outperforming all mutual coupling aware algorithms for small spacings and, hence, systems without decoupling networks are not well-suited for a lossless scenario with small spacings.

Fig. 12 illustrates a more practical scenario with $\gamma = 10^{-2}$ and $d = 0.4$ for different user positions, i.e., angles α_{R_x} . We can see, that for this scenario, the DecoupledBD and the Decoupled method perform very similarly over all user angles. Additionally, the algorithms perform better than in the theoretical case in Fig. 11, however, they are still worse than the Decoupled approach. Moreover, including the effects of mutual coupling by choosing a smaller spacing than $\frac{\lambda}{2}$ increases the performance in comparison to the uncoupled method.

VIII. CONCLUSION

We have seen that the property of the decoupling networks to simplify the structure of the system model with mutual coupling to a structure without mutual coupling leads to new methods and new analytical results. For lossless and very small antenna spacings, the decoupled RISs lead to large performance gains in comparison to uncoupled RISs. Actually,

super-quadratic gains are possible up to a quartic gain in the end-fire direction. Also the BD-RISs are very promising in this ideal scenario, achieving a cubic gain over all user angles. When, considering more realistic assumptions like lossy antenna arrays and larger element spacings (still sub- $\frac{\lambda}{2}$ spacings), the gains are lower but still significantly better than arrays without mutual coupling and a super-quadratic gain can still be observed for certain scenarios. For this more practical considerations, the performance of the BD-RIS and the diagonal RIS with decoupling methods is very similar. Additionally, we have seen that the decoupled RIS outperforms the current state-of-the-art algorithms both w.r.t. performance as well as computational complexity (closed-form solution vs. iterative algorithm). The drawback of the decoupled networks is the increased hardware complexity which will be discussed in future work.

APPENDIX

A. Global Minimum of $f(x)$

We will now derive the global minimum of the function $f_N(x)$ given by

$$f_N(x) = \sum_{n=0}^{N-1} (2n+1)P_n^2(x) > 0 \quad (83)$$

for $x \in [-1, 1]$ and additionally show $f_N(x) \geq \frac{N}{2} \forall x$. It can be directly seen that for $x \pm 1$ the function obtains its maximum and we will exclude these points in the following. By recognizing that $f_N(x)$ is the reciprocal of the Christoffel function for Legendre polynomials, we can rewrite the function with the Christoffel-Darboux formula (see [33, p.43, (3.2.4)]) as

$$f_N(x) = N(P'_N(x)P_{N-1}(x) - P'_{N-1}(x)P_N(x)). \quad (84)$$

By applying [34, Lemma 1], the objective is simplified to

$$f_N(x) = (1-x^2)(P'_N(x))^2 + N^2P_N^2(x) \quad (85)$$

where $P'_N(x)$ is the derivative of $P_N(x)$. By recognizing similarities to the function [33, p.164, Theorem 7.3.1, (7.3.2)] we define the lower bound on the objective

$$g_N(x) = \frac{N}{N+1}(1-x^2)(P'_N(x))^2 + N^2P_N^2(x) \quad (86)$$

and, hence, it holds that

$$f_N(x) \geq g_N(x). \quad (87)$$

According to [33, p.164, Theorem 7.3.1, (7.3.2)], the derivative is given by

$$g'_N(x) = \frac{2N}{N+1}x(P'_N(x))^2. \quad (88)$$

As $g_N(x)$ is monotonically increasing from 0 to ± 1 , it attains its global minimum at $x = 0$. Therefore, we have

$$f_N(x) \geq g_N(x) \geq g_N(0). \quad (89)$$

1) *N even*: We show now that $f_N(x) \geq \frac{N}{2}$ for even N . When N is even we have $P'_N(0) = 0$ and, hence,

$$f_N(0) = g_N(0) = N^2P_N^2(0). \quad (90)$$

Combining this with (89), we can already see that the global minimum of $f_N(x)$ for even N is $x = 0$ as $f_N(0) = g_N(0)$. It remains to show that $P_N^2(0) \geq \frac{1}{2N}$. From [35, p.782, (22.7.10)] we have $N^2P_N^2(0) = (N-1)^2P_{N-2}^2(0)$ for $x = 0$. It follows that

$$P_N^2(0) = \frac{(N-1)^2}{N^2}P_{N-2}^2(0) \geq \frac{(N-1)^2}{2N^2(N-2)} \geq \frac{1}{2N} \quad (91)$$

and with $P_2^2(0) = \frac{1}{4}$ the proof by induction is complete.

2) *N odd*: When N is odd, the function $f_N(x)$ does not attain its global minimum at $x = 0$ (see Section A3) for a discussion). In this case we use the lower bound, which reduces for odd N to

$$f_N(x) \geq g_N(0) = \frac{N}{N+1}(P'_N(0))^2 \quad (92)$$

as $P_N(0) = 0$ for odd N . From [35, p.783, (22.8.5)] we have $(P'_N(0))^2 = N^2P_{N-1}^2(0)$ for $x = 0$. Hence, it follows that

$$g_N(0) = \frac{N}{N+1}N^2P_{N-1}^2(0) \geq \frac{N}{2}. \quad (93)$$

The last step follows from the fact that $N-1$ is even and, hence, $P_{N-1}^2(0) \geq \frac{1}{2(N-1)}$ according to (91).

3) *Global Minimum*: We have already seen that for even N the function attains its global minimum at $x = 0$ with the value $f_N(0) = N^2P_N^2(0)$. For odd N this is not the case which we will shortly discuss. The derivative of the objective can be factorized into

$$f'(x) = 2P'_N(x)b(x), \quad \text{with}$$

$$b(x) = (1-x^2)P''_N(x) - xP'_N(x) + N^2P_N(x).$$

It can be seen that the extrema can be split into the two sets

$$x_+ : b(x_+) = 0, P'_N(x_+) \neq 0 \quad \text{and} \quad (94)$$

$$x_- : P'_N(x_-) = 0. \quad (95)$$

With [35, p.781, 22.6.13; p.783, 22.8.5] it can be shown that

$$b(x) = \frac{N(xP_{N-1}(x) - P_N(x))}{1-x^2} \quad (96)$$

holds and, therefore, $b(x_+) = 0 \iff P_N(x_+) = x_+P_{N-1}(x_+)$. Combining this with the properties of Legendre polynomials [35, p.783, 22.8.5; p.782, 22.7.10; p.783, 22.8.5], it can be further shown that also

$$f''(x_+) = -2(N-1)\frac{(P'_N(x_+))^2}{1-x_+^2} < 0 \quad (97)$$

holds and, hence, all points x_+ are local maxima. As they are all maxima, the points x_+ don't have to be considered for the

global minimum. At the remaining stationary points x_- the function can be written as

$$f_N(x_-) = N^2 P_N^2(x_-) \quad (98)$$

as $P'_N(x_-) = 0$. With $P'_N(x_-) = 0$ and $P_N(x_-) = -P''_N(x_-) \frac{1-x_-^2}{N(N+1)}$ from [35, p.781, 22.6.13] it can be shown that x_- are the maxima of $N^2 P_N^2(x)$ which are increasing from 0 to ± 1 (see [33, p.164, Theorem 7.3.1, (7.3.2)]). Hence, $f(x_-)$ is increasing from 0 to ± 1 . It follows that for even N , the global minimum is $x = 0$ with the function value $f_N(0) = N^2 P_N^2(0)$. For odd N , the global minimum is at $\pm x_0$ where x_0 is the positive zero of $P'_N(x)$ nearest to $x = 0$.

REFERENCES

- [1] D. Semmler, J. A. Nossek, M. Joham, and W. Utschick, "Performance Analysis of Systems with Coupled and Decoupled RISs," in *2024 19th International Symposium on Wireless Communication Systems (ISWCS)*, 2024, pp. 1–6.
- [2] Q. Wu and R. Zhang, "Intelligent Reflecting Surface Enhanced Wireless Network via Joint Active and Passive Beamforming," *IEEE Transactions on Wireless Communications*, vol. 18, no. 11, pp. 5394–5409, 2019.
- [3] M. Di Renzo, A. Zappone, M. Debbah, M.-S. Alouini, C. Yuen, J. de Rosny, and S. Tretyakov, "Smart radio environments empowered by reconfigurable intelligent surfaces: How it works, state of research, and the road ahead," *IEEE Journal on Selected Areas in Communications*, vol. 38, no. 11, pp. 2450–2525, 2020.
- [4] C. Huang, A. Zappone, G. C. Alexandropoulos, M. Debbah, and C. Yuen, "Reconfigurable Intelligent Surfaces for Energy Efficiency in Wireless Communication," *IEEE Transactions on Wireless Communications*, vol. 18, no. 8, pp. 4157–4170, 2019.
- [5] H. Guo, Y.-C. Liang, J. Chen, and E. G. Larsson, "Weighted Sum-Rate Maximization for Reconfigurable Intelligent Surface Aided Wireless Networks," *IEEE Transactions on Wireless Communications*, vol. 19, no. 5, pp. 3064–3076, 2020.
- [6] C. Pan, H. Ren, K. Wang, W. Xu, M. ElKashlan, A. Nallanathan, and L. Hanzo, "Multicell MIMO Communications Relying on Intelligent Reflecting Surfaces," *IEEE Transactions on Wireless Communications*, vol. 19, no. 8, pp. 5218–5233, 2020.
- [7] D. Semmler, M. Joham, and W. Utschick, "High SNR Analysis of RIS-Aided MIMO Broadcast Channels," in *2023 IEEE 24th International Workshop on Signal Processing Advances in Wireless Communications (SPAWC)*, 2023, pp. 221–225.
- [8] S. Zhang and R. Zhang, "Capacity Characterization for Intelligent Reflecting Surface Aided MIMO Communication," *IEEE Journal on Selected Areas in Communications*, vol. 38, no. 8, pp. 1823–1838, 2020.
- [9] D. Semmler, M. Joham, and W. Utschick, "A Zero-Forcing Approach for the RIS-Aided MIMO Broadcast Channel," in *ICC 2024 - IEEE International Conference on Communications*, 2024, pp. 4378–4383.
- [10] S. Syed, D. Semmler, D. B. Amor, M. Joham, and W. Utschick, "Design of a Single-User RIS-Aided MISO System Based on Statistical Channel Knowledge," in *2023 57th Asilomar Conference on Signals, Systems, and Computers*, 2023, pp. 460–464.
- [11] Y. Han, W. Tang, S. Jin, C.-K. Wen, and X. Ma, "Large Intelligent Surface-Assisted Wireless Communication Exploiting Statistical CSI," *IEEE Transactions on Vehicular Technology*, vol. 68, no. 8, pp. 8238–8242, 2019.
- [12] M.-M. Zhao, Q. Wu, M.-J. Zhao, and R. Zhang, "Intelligent Reflecting Surface Enhanced Wireless Networks: Two-Timescale Beamforming Optimization," *IEEE Transactions on Wireless Communications*, vol. 20, no. 1, pp. 2–17, 2021.
- [13] J. Xu, Y. Liu, X. Mu, and O. A. Dobre, "STAR-RISs: Simultaneous Transmitting and Reflecting Reconfigurable Intelligent Surfaces," *IEEE Communications Letters*, vol. 25, no. 9, pp. 3134–3138, 2021.
- [14] Y. Liu, X. Mu, J. Xu, R. Schober, Y. Hao, H. V. Poor, and L. Hanzo, "STAR: Simultaneous Transmission and Reflection for 360° Coverage by Intelligent Surfaces," *IEEE Wireless Communications*, vol. 28, no. 6, pp. 102–109, 2021.
- [15] Z. Zhang, L. Dai, X. Chen, C. Liu, F. Yang, R. Schober, and H. V. Poor, "Active RIS vs. Passive RIS: Which Will Prevail in 6G?" *IEEE Transactions on Communications*, vol. 71, no. 3, pp. 1707–1725, 2023.
- [16] C. You and R. Zhang, "Wireless Communication Aided by Intelligent Reflecting Surface: Active or Passive?" *IEEE Wireless Communications Letters*, vol. 10, no. 12, pp. 2659–2663, 2021.
- [17] S. Shen, B. Clerckx, and R. Murch, "Modeling and architecture design of reconfigurable intelligent surfaces using scattering parameter network analysis," *IEEE Transactions on Wireless Communications*, vol. 21, no. 2, pp. 1229–1243, 2022.
- [18] M. Nerini, S. Shen, and B. Clerckx, "Closed-Form Global Optimization of Beyond Diagonal Reconfigurable Intelligent Surfaces," *IEEE Transactions on Wireless Communications*, vol. 23, no. 2, pp. 1037–1051, 2024.
- [19] H. Li, S. Shen, and B. Clerckx, "Beyond Diagonal Reconfigurable Intelligent Surfaces: From Transmitting and Reflecting Modes to Single-, Group-, and Fully-Connected Architectures," *IEEE Transactions on Wireless Communications*, vol. 22, no. 4, pp. 2311–2324, 2023.
- [20] J. A. Nossek, D. Semmler, M. Joham, and W. Utschick, "Physically Consistent Modeling of Wireless Links With Reconfigurable Intelligent Surfaces Using Multiport Network Analysis," *IEEE Wireless Communications Letters*, vol. 13, no. 8, pp. 2240–2244, 2024.
- [21] G. Gradoni and M. Di Renzo, "End-to-end mutual coupling aware communication model for reconfigurable intelligent surfaces: An electromagnetic-compliant approach based on mutual impedances," *IEEE Wireless Communications Letters*, vol. 10, no. 5, pp. 938–942, 2021.
- [22] M. T. Ivrlač and J. A. Nossek, "Toward a circuit theory of communication," *IEEE Transactions on Circuits and Systems I: Regular Papers*, vol. 57, no. 7, pp. 1663–1683, 2010.
- [23] H. Li, S. Shen, M. Nerini, M. Di Renzo, and B. Clerckx, "Beyond Diagonal Reconfigurable Intelligent Surfaces With Mutual Coupling: Modeling and Optimization," *IEEE Communications Letters*, vol. 28, no. 4, pp. 937–941, 2024.
- [24] A. Abrardo, A. Toccafondi, and M. Di Renzo, "Design of Reconfigurable Intelligent Surfaces by Using S-Parameter Multiport Network Theory—Optimization and Full-Wave Validation," *IEEE Transactions on Wireless Communications*, vol. 23, no. 11, pp. 17 084–17 102, 2024.
- [25] M. Nerini, S. Shen, H. Li, M. Di Renzo, and B. Clerckx, "A Universal Framework for Multiport Network Analysis of Reconfigurable Intelligent Surfaces," *IEEE Transactions on Wireless Communications*, vol. 23, no. 10, pp. 14 575–14 590, 2024.
- [26] J. A. Nossek, D. Semmler, M. Joham, and W. Utschick, "Modelling of Wireless Links with Reconfigurable Intelligent Surfaces Using Multiport Network Analysis," in *2024 27th International Workshop on Smart Antennas (WSA)*, 2024, pp. 1–8.
- [27] X. Qian and M. D. Renzo, "Mutual Coupling and Unit Cell Aware Optimization for Reconfigurable Intelligent Surfaces," *IEEE Wireless Communications Letters*, vol. 10, no. 6, pp. 1183–1187, 2021.
- [28] A. Abrardo, D. Dardari, M. Di Renzo, and X. Qian, "MIMO Interference Channels Assisted by Reconfigurable Intelligent Surfaces: Mutual Coupling Aware Sum-Rate Optimization Based on a Mutual Impedance Channel Model," *IEEE Wireless Communications Letters*, vol. 10, no. 12, pp. 2624–2628, 2021.
- [29] M. Akrouf, F. Bellili, A. Mezghani, and J. A. Nossek, "Physically Consistent Models for Intelligent Reflective Surface-assisted Communications under Mutual Coupling and Element Size Constraint," *arXiv 2302.11130*, 2023.
- [30] H. E. Hassani, X. Qian, S. Jeong, N. S. Perović, M. Di Renzo, P. Mursia, V. Sciancalepore, and X. Costa-Pérez, "Optimization of RIS-Aided MIMO—A Mutually Coupled Loaded Wire Dipole Model," *IEEE Wireless Communications Letters*, vol. 13, no. 3, pp. 726–730, 2024.
- [31] M. Nerini, H. Li, and B. Clerckx, "Global Optimal Closed-Form Solutions for Intelligent Surfaces With Mutual Coupling: Is Mutual Coupling Detrimental or Beneficial?" 2024. [Online]. Available: <https://arxiv.org/abs/2411.04949>
- [32] E. Altshuler, T. O'Donnell, A. Yaghjian, and S. Best, "A monopole superdirective array," *IEEE Transactions on Antennas and Propagation*, vol. 53, no. 8, pp. 2653–2661, 2005.
- [33] G. Szegő, *Orthogonal Polynomials*. Providence, RI: American Mathematical Society, 1975.
- [34] L. Bos, A. Narayan, N. Levenberg, and F. Piazzon, "An Orthogonality Property of the Legendre Polynomials," *Constructive Approximation*, 2017.
- [35] M. Abramowitz and I. A. Stegun, Eds., *Handbook of Mathematical Functions with Formulas, Graphs and Mathematical Tables*. New York: Dover Publications, Inc., 1965.